

A systematic study of the inner rotation curves of galaxies observed as part of the GASS and COLD GASS surveys

Guinevere Kauffmann^{1*}, Mei-Ling Huang¹, Sean Moran², Timothy M. Heckman³

¹*Max-Planck Institut für Astrophysik, 85741 Garching, Germany*

²*Harvard-Smithsonian Center for Astrophysics, 60 Garden Street, Cambridge, MA 02138, USA*

³*Department of Physics & Astronomy, Johns Hopkins University, Baltimore, MD, 21218, USA*

23 March 2015

ABSTRACT

We present a systematic analysis of the rotation curves of 187 galaxies with masses greater than $10^{10} M_{\odot}$, with atomic gas masses from the GALEX Arcicibo Sloan Survey (GASS), and with follow-up long-slit spectroscopy from the MMT. Our analysis focuses on stellar rotation curves derived by fitting stellar template spectra to the galaxy spectra binned along the slit. In this way, we are able to obtain accurate rotation velocity measurements for a factor of 2 more galaxies than possible with the H α line. Galaxies with high atomic gas mass fractions are the most dark-matter dominated galaxies in our sample and have dark matter halo density profiles that are well fit by Navarro, Frenk & White profiles with an average concentration parameter of 10. The inner slopes and of the rotation curves correlate more strongly with stellar population age than with galaxy mass or structural parameters. At fixed stellar mass, the rotation curves of more actively star-forming galaxies have steeper inner slopes than less actively star-forming galaxies. The ratio between the galaxy specific angular momentum and the total specific angular momentum of its dark matter halo, R_j , correlates strongly with galaxy mass, structure and gas content. Low mass, disk-dominated galaxies with atomic gas mass fractions greater than 20% have median values of R_j of around 1, but massive, bulge-dominated galaxies have $R_j = 0.2 - 0.3$. We argue that these trends can be understood in a picture where gas inflows triggered by disk instabilities lead to the formation of passive, bulge-dominated galaxies with low specific angular momentum.

Key words: galaxies:haloes; galaxies: formation; galaxies: structure ; galaxies: stellar content

1 INTRODUCTION

Rotation curves are an important probe of the distribution of both the luminous and the dark matter mass in galaxies. They have been studied since the 1970’s primarily as a way to constrain the density profiles of the dark matter halos that are thought to surround all galaxies. Because dark matter increasingly dominates the mass distribution at large distances from the centre of a galaxy, most observational studies have focused on rotation curves measured using the HI line at 21 cm wavelengths. This is because the atomic gas in galaxies generally extends significantly further out than the stars. Many galaxies, however, have holes in the HI distribution at small radii, so if one wishes to measure the shape of the dark matter potential over a wide range of scales, the HI data needs to be complemented by rotation measurements

from optical H α or CO mm line data (see Sofue & Rubin 2001; Combes 2002 for comprehensive reviews).

There is a significantly smaller body of work on the statistical properties of rotation curves. Persic et al. (1996) compiled 1100 rotation curves of spiral galaxies and claimed that a single functional form with galaxy luminosity as the only parameter could provide a “universal” description. The most luminous galaxies show slightly declining rotation curves in the outer part, following a maximum in the disk. Intermediate galaxies have nearly flat rotation curves across the disk. The least luminous galaxies have monotonically increasing rotation curves across their whole disk. These results led Persic et al (1996) to conclude that the dark-to-luminous mass ratio increases with decreasing galaxy luminosity and mass. Later studies of early-type disc galaxies (S0-Sab) by Sofue et al (1999) and Noordermeer et al (2006) revealed large discrepancies with the rotation curves predicted by the Persic et al. fitting formula. These authors

* E-mail: gamk@mpa-garching.mpg.de

found that the shape of the rotation curve depends on the bulge-to-disk ratio of the galaxy; galaxies with concentrated light distributions and larger bulges reach their maximum rotation velocities at smaller radii than galaxies with smaller bulges and more diffuse light distributions.

One limitation of past statistical studies is that because they rely on H α , HI or CO line data, they are biased to galaxies with high gas content and/or ongoing star formation. In principle, galaxy rotation curves can also be derived from stellar absorption lines, but this requires high signal-to-noise spectra and accurate fitting of stellar templates in order to accurately measure shifts in velocity along the slit. In recent years, this has become possible thanks to the increasing efficiency of optical spectrographs and the availability of high resolution stellar template spectra spanning a wide range in wavelength (e.g. Martinsson et al 2013a).

Moran et al. (2012) presented long-slit spectroscopy of 174 galaxies drawn from the GALEX Arecibo Sloan Digital Sky Survey (SDSS)(GASS; Catinella et al. 2010), which was designed to measure the neutral hydrogen content of a representative sample of ~ 1000 galaxies with stellar masses larger than $10^{10} M_{\odot}$ and redshifts $0.02 < z < 0.05$ uniformly selected from the SDSS (York et al. 2000) and Galaxy Evolution Explorer (GALEX; Martin et al 2005) imaging surveys. GASS observations detect HI down to a gas fraction limit of $\sim 3\%$. A companion project on the IRAM 30m telescope, COLD GASS (Saintonge et al 2011), has obtained CO (1-0) line measurements and molecular gas masses for a subset of these galaxies. In addition, a variety of stellar population and structural parameters derived from GALEX/SDSS imaging and spectroscopy are available for the full sample.

This paper presents a systematic analysis of the rotation curves derived from the final sample of 236 longslit spectra obtained over the period from October 2008 to April 2012 using both the Blue Channel Spectrograph on the 6.5m MMT telescope and the Dual Imaging Spectrograph on the 3.5m telescope at Apache Point Observatory (APO). As part of the procedure for measuring SFR and gas-phase metallicity profiles for the galaxies in the sample, Moran et al (2012) derived both stellar rotation curves from fitting template stellar absorption line spectra to the galaxy spectra binned along the slit, and H α rotation curves from fitting Gaussian profiles to the H α emission line after subtraction of the best-fit spectrum.

As we will show, the agreement between the H α and stellar rotation measurements are generally good to within 10-20% in galaxies where both can be accurately determined. We are able to obtain accurate stellar rotation velocity measurements for a factor of 2 more galaxies than is possible with H α alone (187 out of 236 galaxies), permitting a much wider exploration of galaxy parameter space. The stellar rotation curves generally do not extend beyond $\sim 2.5 R_e$ and thus do not in general sample the flat part of the rotation curve with high accuracy. Nevertheless, we will show that we can still use them as probes of, a) the inner mass distribution of the galaxy, b) the radius at which dark matter begins to dominate over baryons (stars and gas), c) the angular momentum content of the galaxy as parametrized by the spin parameter λ . After presenting our data analysis methodology in Section 2, we examine how these three quantities depend on a variety of galaxy properties in Section 3. In Section 4, we select a subset of galaxies where dark

matter dominates well within the optical radius, and we examine constraints on the shape of the dark matter density profile. In section 5, we summarize and conclude. We adopt a Hubble constant of $H_0 = 70 \text{ km s}^{-1} \text{ Mpc}^{-1}$ throughout the paper.

2 DATA ANALYSIS METHODOLOGY

2.1 Rotation curve estimation and sample selection

The procedure for measuring rotation curves is described in detail in Moran et al (2010). Working outwards from the galaxy centre, each spectrum is binned spatially to achieve a signal-to-noise of at least 6 (\AA^{-1}) in each bin, the minimum needed for a reliable velocity estimate. For each binned spectrum, the effective spatial position is determined by calculating the luminosity-weighted average radius of all spatial positions that entered the co-add.

The radial velocity as a function of radius is measured in two ways: 1) by cross-correlating each spectrum against superpositions of template spectra from Bruzual & Charlot (2003) stellar population synthesis models to determine the velocity, 2) by fitting directly for the centroids of the H α emission lines. The methods yield generally consistent curves at radii where we can fit templates and measure emission line centroids. This is shown in Figure 1, where we show plots of the difference between the velocity determined by fitting stellar templates (V_{abs}) and the velocity inferred from the shift of the centroid of the H α line ($V_{H\alpha}$). The velocity differences are normalized by dividing by $0.5(V_{abs} + V_{H\alpha})$ to yield a *fractional* difference. We compute the average fractional distance for each galaxy with where V_{abs} and $V_{H\alpha}$ are both well-measured over at least 10 spectral bins, and we plot this quantity as a function of different global galaxy parameters in each panel of Figure 1.

As can be seen, $V_{H\alpha}$ is generally larger than V_{abs} , but this is a small effect (10% systematic effect on average). A similar effect was found by Martinsson et al (2013a), which these authors attributed to “asymmetric drift”, i.e. the fact that stars can be supported against gravitational collapse by both rotation and by random motions. If this is the case, one might expect the average velocity difference to correlate strongly with the bulge-to-disk ratio of the galaxy, and for the velocity difference to get systematically larger in the inner regions of the galaxy. We can explore this hypothesis by plotting the velocity difference as a function of Σ_* for each spectral bin, where Σ_* is the local stellar surface mass density of stars measured from our derived stellar mass profiles. This is shown in Figure 2. Black points show the fractional difference between $V_{H\alpha}$ and V_{abs} for individual spectral bins, while the red squares show the average value of the fractional offset in fixed bins of Σ_* . As can be seen, the average fractional offset increases from 0.03 at stellar surface densities less than $10^8 M_{\odot} \text{ kpc}^{-2}$ to 0.15 at stellar surface densities of $10^9 M_{\odot} \text{ kpc}^{-2}$, which is consistent with the “asymmetric drift” hypothesis. The bottom panels of Figure 1 show that the largest velocity differences averaged over the rotation curves of individual galaxies occur for galaxies with red NUV-r colours and high inclinations. This might be caused by dust extinction effects or systematic errors in the measurement of the centroid of the H α when the signal-to-noise

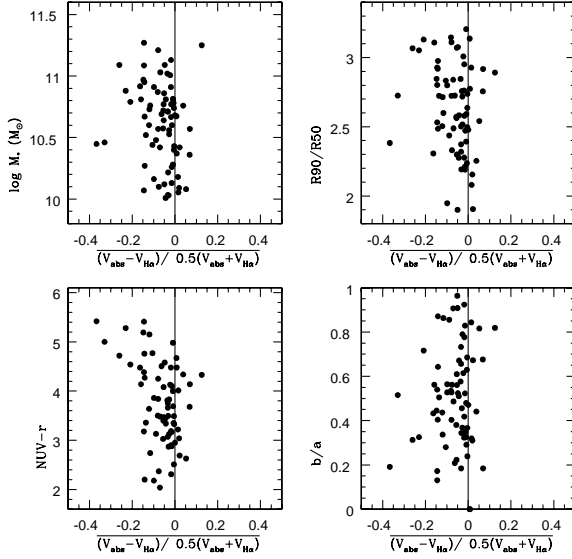


Figure 1. The mean fractional difference between the velocity estimated by fitting stellar templates to the longslit spectra (V_{abs}) and by fitting to the centroid of the $H\alpha$ emission line ($V_{H\alpha}$) is plotted as a function of different global galaxy parameters in each panel: stellar mass (top left), r -band concentration parameter (top right), global NUV- r colour (bottom left), and axial ratio (bottom right).

is low. In either case we expect the stellar rotation measurements to be more reliable. In what follows, we will analyze the stellar rotation curves without attempting to correct for asymmetric drift or extinction effects, which would require more detailed modelling.

We proceed to inspect each of the 236 stellar rotation curves by eye and we select those that have measured velocities with fractional errors less than 20% across a significant portion of the optical disk and those that are regular enough to fit with a smooth function of the form

$$V(R) = V_{max}R/(R^\alpha + r_s^\alpha)^{1/\alpha} + \Delta V \quad (1)$$

(Böhm et al. 2004; Moran et al 2007,2010), where R is the radius, α and r_s are free parameters that govern the shape of the rotation curve, and ΔV is the offset of the galaxy’s central velocity from the redshift obtained from the SDSS spectrum (also left as a free parameter). This results in a sample of 187 galaxies, of which 89 (i.e. around a half) also have $H\alpha$ rotation curves measured over the same radii as the stellar rotation curves. The properties of this sample are shown in Figure 3. The black histograms show the stellar mass, concentration index and NUV- r colour distributions of the selected sample of 187 galaxies, while the red histograms are for the galaxies where the rotation curves were either very poorly measured or too irregular to work with. As can be seen, the selected sample of 187 galaxies with good stellar rotation curves spans a wide range in stellar mass, concentration and colour; only the very most massive ($M_* > 10^{11}M_\odot$), reddest (NUV- $r > 6$) and most concentrated ($R_{90}/R_{50} > 3.25$) galaxies are systematically excluded.

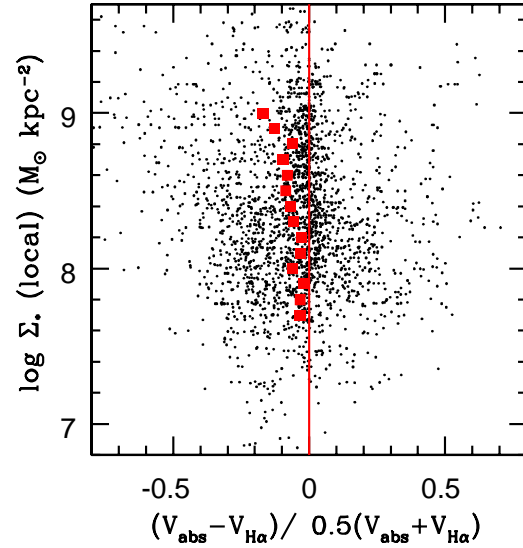


Figure 2. The fractional difference between the velocity estimated by fitting stellar templates to the longslit spectra (V_{abs}) and by fitting to the centroid of the $H\alpha$ emission line ($V_{H\alpha}$) is plotted as a function of local stellar mass surface density Σ_* . Black points show results for individual spectral bins, while red squares show the average value of the fractional difference as a function of Σ_* .

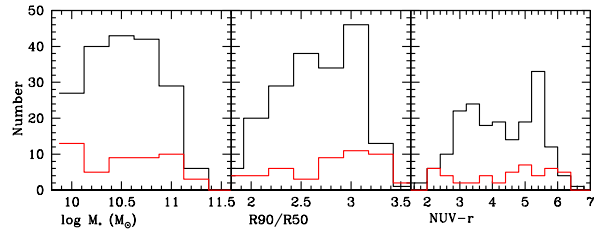


Figure 3. The black histograms show the distribution of the number of galaxies as a function of stellar mass (left), concentration parameter (middle) and NUV- r colour (right) for our selected sample of 187 galaxies with well-measured, regular stellar rotation curves. The red histograms show the distributions for the 49 galaxies where stellar rotation curves could not be accurately determined, or where the rotation curves were too irregular to fit a function of the form given in the text.

2.2 Parameters derived from the rotation curves

Our stellar rotation curves are well-determined out to radii of between 7 and 20 kpc. This is generally not far out enough in the disk to measure the shape of the outer rotation curve, but we are able to accurately measure the inner slope and determine whether the gravitational potential is dominated by baryons (stars+gas) or by dark matter over the optical radius of the disk. In addition, as we will discuss, we measure the total angular momentum content of the stellar disk, as parameterized by the spin parameter λ .

(i) *The inner slope* is defined to be the slope of the best-fit linear relation between V_{abs} and R , evaluated from the center of the galaxy out to a radius of $\pm r_s$, where r_s is the fitting parameter in equation (1). The inner slope provides a measure of the shear in the central regions of the galaxy. In order to be able to compare massive galaxies with less massive galaxies in a meaningful way, we scale the velocities by dividing by V_{max} , where V_{max} is an estimate of the maximum rotation velocity of the galaxy. We also scale the radii R the radii by dividing by R_{50} , where R_{50} is the radius containing half the total r-band light of the galaxy. Because the errors on the fitted value of V_{max} in equation (1) are large for galaxies where the outer regions of the rotation curve are not very well sampled, we estimate V_{max} using the baryonic Tully-Fisher relation given in Catinella et al (2012) ($\log V_{max} = 0.237 \log x - 0.251$; $x = M_* + 1.4M_{HI}$).

(ii) *The dark-matter domination radius* $R_{50}(DM)$ is defined as the radius where the enclosed dark matter mass exceeds the total baryonic mass. The total mass enclosed within radius R can be estimated directly from the rotation curve after correction for inclination effects. The inclination of the galaxy is estimated using its r -band axial ratio b/a as $\cos i = b/a$. The total baryonic mass enclosed within radius R is the sum of the stellar and gas mass within this radius. Stellar mass-to-light profiles for each of the galaxies in our sample are derived by fitting SDSS 5-band optical photometry to stellar population synthesis model grids using standard techniques (see for example Salim et al 2005). The mass-to-light ratio will depend on the assumed initial mass function (IMF). For simplicity, we have assumed a fixed Chabrier (2003) form.

Because we only have single-dish measurements of the 21cm and CO(1-0) lines, the gas mass within radius R must be approximated using assumed profiles. It has been known for some time that there is a tight relation between the characteristic size of the HI disk $D1$ and the total HI mass in the disk (Broeils & Rhee 1997),

$$\log M_{HI} = 1.96 \log D1 + 6.52, \quad (2)$$

where $D1$ is defined as the diameter where the face-on corrected angular-averaged HI column density reaches $1 M_\odot \text{pc}^{-2}$ (corresponding to $1.25 \times 10^{20} \text{atoms cm}^{-2}$). This relation has recently been demonstrated to extend up to total HI masses of $2 \times 10^{10} M_\odot$ and disk diameters of 100 kpc (Wang et al 2013). Wang et al (2014) show that a simple analytic expression of the form

$$\Sigma_{HI}(r) = \frac{I_1 \exp(-r/r_s)}{1 + I_2 * \exp(-r/r_c)}, \quad (3)$$

where I_1 , I_2 , r_s and r_c are free parameters, can provide an excellent description of the HI density profiles of nearby gas-rich and normal spiral galaxies. Bigiel & Blitz (2012) show that total (atomic+molecular) gas profiles are well-characterized by a function of the form

$$\Sigma_{gas}/\Sigma_{transit} = 2.1e^{-1.65r/R_{25}} \quad (4)$$

where $\Sigma_{transit}$ is the radius where the atomic gas surface density equals the molecular gas surface density, and R_{25} is the optical radius of the galaxy.

We construct atomic and molecular gas surface density profiles for the galaxies in our sample as follows. Equation (2) allows us to specify $D1$, given the observed total HI mass

of the galaxy. Figure 6 of Wang et al (2014) shows that $r_s/R1 = r_s/(0.5D1)$ lies in the range 0.15 to 0.3. Also based on this data, we allow r_c to range from $0.05r_s$ to $0.7r_s$. Finally, we also require that $\int 2\pi\Sigma_{HI}(r)rdr = M_{HI}$. We first generate a family of HI profiles that satisfy these constraints. If the galaxy has detected molecular gas, then we add in molecular gas at each radius such that equation (4) is satisfied and we only keep those profiles where the integral over the resulting molecular gas profile yields a value close to the observed total H_2 mass. Finally we add each acceptable gas profile to the stellar profile and compute $R_{50}(DM)$ as the value averaged over each $\Sigma_*(r) + \Sigma_{gas}(r)$ combination. In practice, because stars dominate the baryonic mass budget for the majority of the galaxies in our sample, the uncertainty in $R_{50}(DM)$ arising from the variety of acceptable gas profiles is small, typically 10-20 %.

(iii) *The spin parameter* λ . Observational measurements of the specific angular momentum in galaxies place constraints on the way galaxies acquire their mass and angular momentum. The specific angular momentum is often parametrized in terms of a dimensionless spin parameter λ . Here, we adopt the definition of galaxy spin parameter given in equation (2) of Dutton & Van den Bosch (2012)

$$\lambda_{gal} = \frac{(J_{gal}/M_{gal})}{\sqrt{2}R_{vir}V_{vir}}, \quad (5)$$

where J_{gal} is the total angular momentum of the galaxy, M_{gal} is the total baryonic mass of the galaxy, and R_{vir} and V_{vir} are the radius and circular velocity of its dark matter halo. As discussed by Dutton & Van den Bosch (2012), if λ_{gal} can be measured for a representative set of galaxies, the angular momentum ratio R_j , defined as the ratio between the galaxy specific angular momentum and the specific angular momentum of the halo,

$$R_j = \frac{(J_{gal}/M_{gal})}{(J_{vir}/M_{vir})} = \frac{\lambda_{gal}}{\lambda_{halo}}, \quad (6)$$

can then be constrained. The distribution of λ_{halo} has been extensively studied using N-body simulations (e.g. Bett et al 2007) and semi-analytic models of disk galaxy formation (e.g. Fu et al 2010, Guo et al 2011) typically *assume* that $R_j = 1$, because this leads to good agreement with the observed sizes of galaxies. In this paper, we examine the validity of this assumption.

Calculating the total angular momentum for each galaxy in our sample, given its rotation curve and baryonic mass density profile is straightforward:

$$J_{gal} = 2\pi \int (\Sigma_*(r) + \Sigma_{gas}(r))V_{rot}(r)rdr, \quad (7)$$

Accurate estimates of R_{vir} and V_{vir} cannot be made for individual galaxies in our sample. Instead, we adopt the parameterized relation between galaxy stellar mass and dark matter halo mass at $z = 0$ derived using the galaxy abundance-matching technique in Moster et al (2013),

$$M_*/M_{halo} = 2N [(M_{halo}/M_1)^{-\beta} + (M_{halo}/M_1)^\gamma]^{-1}, \quad (8)$$

with $N = 0.035$, $M_1 = 3 \times 10^{11} M_\odot$, $\beta = 1.5$ and $\gamma = 0.6$. The virial radius R_{vir} can then be computed from the relation $M_{halo} = 200\rho_{crit}(4\pi/3)R_{vir}^3$, where ρ_{crit} is the critical density of the universe, and V_{vir} is given by $V_{vir} = (GM_{halo}/R_{vir})^{1/2}$.

3 RESULTS

3.1 Inner slope and core radius trends

In Figure 4, we show plots of the inner slope (with velocity scaled by V_{max} as described in the previous section, and radius scaled by the half-light radius of the galaxy R_{50}), as functions of a variety of different global galaxy parameters. Black points show inner slope values measured for individual galaxies, while red squares show the running median. We have binned the points along the x-axis such that there are always 12 galaxies in each bin, and the errorbar on the median value of the slope is calculated by boot-strap resampling the galaxies in each bin.

As can be seen from the first two panels, there is no significant trend in inner slope as a function of the stellar mass or stellar velocity dispersion of the galaxy. The inner slope also does not appear to vary as a function of galaxy structural parameters such as the stellar surface mass density or the concentration index of the light. The inner slope is, however, quite strongly correlated with parameters describing the age of the stellar populations and the gas content of the galaxy. We note that the detailed behaviour of this trend is different for each of the 5 parameters we plot. A roughly continuous trend is seen as a function of the global NUV-r colour, with the bluest galaxies exhibiting inner slopes that are twice as steep as the reddest galaxies. For other parameters such as atomic and molecular gas mass fraction, specific star formation rate and 4000 Å break strength, no dependence is seen for the gas-poor/old galaxy population, but a dependence does set in at higher gas mass fractions and at young ages. The 4000 Å break index $D_n(4000)$ and the specific star formation rate SFR/M_* are both measured within the 3 arcsecond SDSS fibre aperture and hence probe the stellar populations in the very central regions of the galaxy. As can be seen in the last two panels, there is again a *decrease* in inner slope for galaxies with the very youngest central stellar populations.

In Figure 5, we plot our galaxies in the two-dimensional planes of stellar surface mass density, concentration index, NUV-r colour and 4000 Å break strength versus stellar mass, and we colour-code each point according to the value of the inner slope: cyan points correspond to inner slope values of less than 0.05, black points to inner slopes in the range 0.05 to 0.2, and magenta points to inner slopes greater than 0.2. In agreement with the results shown in Figure 4, the galaxies with small and large inner slopes separate most clearly in NUV-r and $D_n(4000)$. However, in this plot we also see that at fixed colour, stellar surface density or concentration index, galaxies with steep inner slopes are more massive than galaxies with flat inner slopes. This plot helps us to understand results in the literature (e.g. Persic et al 1996), which strongly emphasize the dependence of rotation curve shape on galaxy luminosity or mass. The strong trend with colour will only be found in samples like ours that include weakly star-forming and early-type galaxies.

A quantity that is closely related to the inner slope is the radius r_s , defined in equation (1). This is the radius where the rotation curve flattens away from the inner power-law inner region. We note that our definition of the inner slope of the rotation curve is mainly controlled by variations in the quantity r_s/R_{50} , because $\Delta V_c/V_{max}$ is generally ~ 1 . r_s can be regarded as the “core radius” of the sum

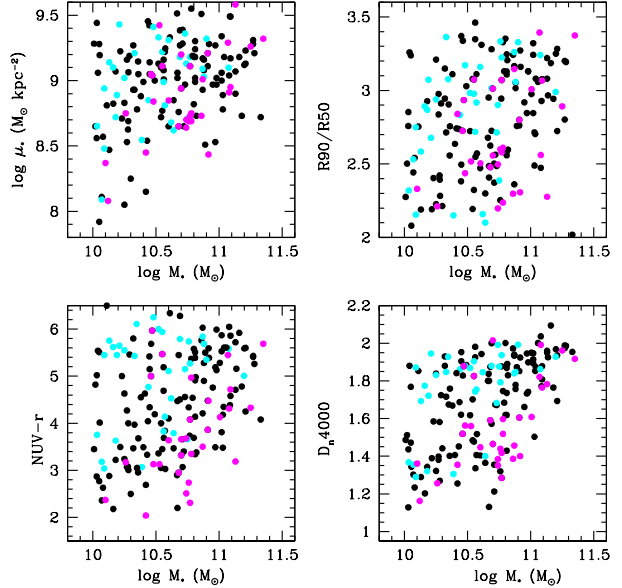


Figure 5. Galaxies are plotted in the two-dimensional planes of stellar surface mass density, concentration index, NUV-r colour and 4000 Å break strength versus stellar mass. Each point is colour-coded according to the value of the inner slope: cyan points correspond to inner slope values of less than 0.05, black points to inner slopes in the range 0.05 to 0.2, and magenta points to inner slopes greater than 0.2.

of the dark matter halo and stellar density profiles. Our results imply that blue, star-forming galaxies have *total mass distributions* with smaller core radii than red, passive galaxies. We note that previous work (e.g. Kormendy & Freeman 2004; Spano et al 2008; Donato et al 2009) has focused on the inferred core radii dark matter halos after subtracting the contribution from the stars and gas. As we have already discussed, most of the galaxies in our sample are gravitationally dominated by baryons in their inner regions, so we will not attempt such a decomposition for the whole sample, only for the subset which are dark matter dominated within R_{50} .

3.2 The dark-matter domination radius

We are able to follow rotation curve out to large enough radius for 103 out of the 187 galaxies in our sample to measure the radius $R_{50}(DM)$ where the dark matter first contributes more than half the mass interior to that radius. The properties of this subset of galaxies are shown in Figure 6. Black histograms show distributions of stellar mass, stellar surface mass density, concentration index, 4000 Å break strength, colour and atomic gas mass fraction for all the galaxies where we are able to estimate $R_{50}(DM)$, while red histograms show the distributions of these properties for galaxies where we do not trace the rotation curve far enough to make an estimate of this quantity. As can be seen, the lowest mass galaxies with $M_* < 2 \times 10^{10} M_\odot$ are missing from the sample with measured $R_{50}(DM)$, but otherwise the sample covers a wide range in colour and structural properties.

Figure 7 shows how a variety of galaxy parameters cor-

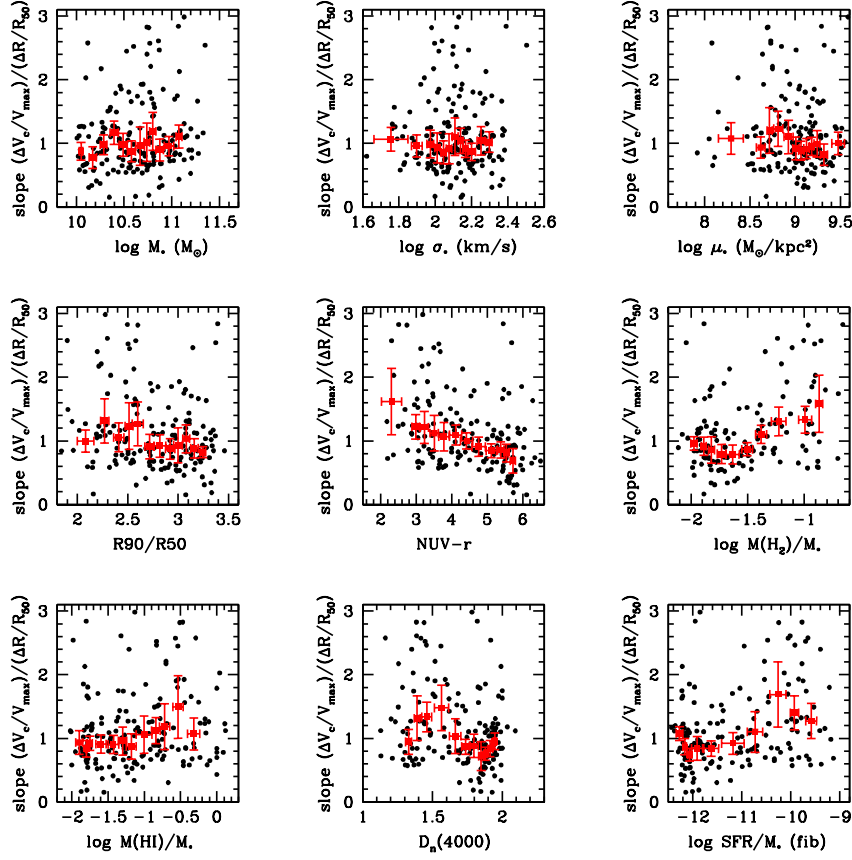


Figure 4. The inner slope of the rotation curve (see text) is plotted as a function of (from left-to-right and from top-to-bottom) a) stellar mass M_* , b) stellar velocity dispersion measured from the SDSS spectrum, c) stellar mass surface density μ_* , d) concentration index, e) NUV-r colour, f) molecular gas mass fraction, g) atomic gas mass fraction, h) 4000 Å break strength, i) specific star formation measured within the SDSS fibre. Black points show inner slope values measured for individual galaxies, while red squares show the running median. We have binned the points along the x-axis such that there are always 12 galaxies in each bin, and the errorbar on the median value of the slope is calculated by boot-strap resampling the galaxies in each bin.

relate with $R_{50}(DM)$. Once again, we find weak correlations with galaxy mass and structural parameters and stronger correlations with galaxy colour and gas content. The two bottom panels of the figure show the parameters that correlate best with the dark matter domination radius: the global NUV-r colour and the atomic gas mass fraction. As can be seen, the majority of galaxies with atomic gas mass fractions greater than 0.1 and NUV-r colours less than 4 become dark matter-dominated within $2R_{50}$. Galaxies with less than a few percent atomic gas and NUV-r > 5 become dark matter dominated at radii larger than $2R_{50}$.

3.3 Spin parameter

In Figure 8, we show plots of the differential (left) and cumulative (right) distributions of derived spin parameters for all 187 galaxies with well-measured rotation curves in our sample. We are able to use the full sample, because in general, the stellar rotation curves can be accurately determined over most of the optical radius of the disk. As can be seen, the median value of λ is 0.01 and the $\pm 1\sigma$ range in λ ex-

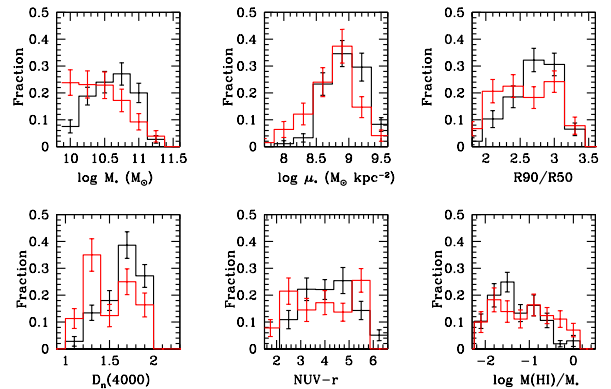


Figure 6. Black histograms show the distribution of properties of the subset of 103 galaxies for which we are able to estimate the dark matter domination radius, while red histograms show the distribution of the properties of galaxies where the rotation curve does not extend far enough.

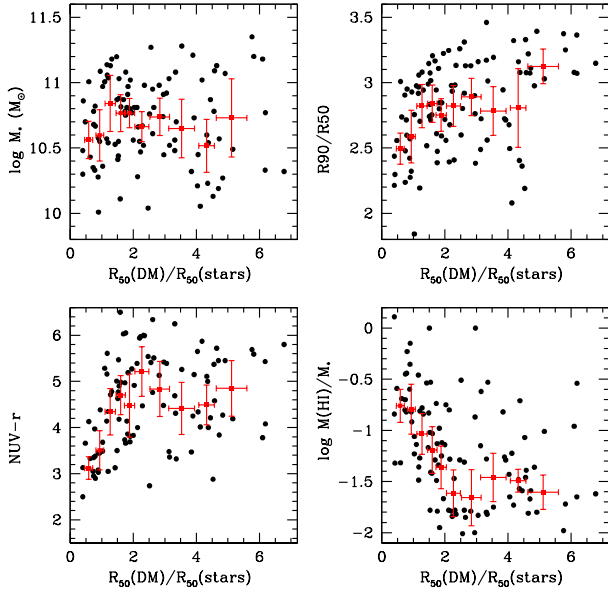


Figure 7. The stellar masses, concentration indices, NUV- r colours and atomic gas mass fractions are plotted as a function of the dark matter-domination radius $R_{50}(DM)$. Black points show parameter values for individual galaxies, while red squares show the running median of each parameter at fixed $R_{50}(DM)$. We have binned the points along the x-axis such that there are always 12 galaxies in each bin, and the errorbar on the median is calculated by boot-strap resampling the galaxies in each bin.

tends from 0.003 to 0.03. The observed median is a factor 3-4 lower than the median value of the spin parameters of dark matter halo measured in N-body simulations of structure formation in a Λ CDM cosmology (e.g. Maccio et al 2007) and the 1σ scatter is about twice as large as found in simulations. Our results are consistent with the conclusions presented in Dutton & Van den Bosch (2012). These authors inferred spin parameter distributions indirectly using ensembles of bulge+disk+halo models that were tuned to fit observational constraints such as the Tully-Fisher relation, the disk size versus stellar mass relation, and the relation between stellar and dark matter halo mass. Based on this analysis, Dutton & Van den Bosch (2012) inferred that the average value of λ for disk galaxies was 0.019 and that galaxy spin did not correlate with halo mass. The big advantage of deriving the spin parameter directly from the observed rotation curve of the galaxy, is that we are able to examine correlations of λ with different galaxy parameters.

In Figure 9, we plot λ as a function of galaxy stellar mass, concentration index, atomic gas mass fraction and 4000 Å break index strength. Once again, black dots show results for individual galaxies, while the red line shows the running median. The spin parameter correlates with all of the plotted parameters. Low mass, low concentration, gas-rich galaxies with young stellar populations have larger spin parameters than high mass, high concentration, gas-poor galaxies with old stellar populations. This is not unexpected since it is believed that the formation of bulge-dominated (early-type) galaxies involves processes such as interactions or mergers, which cause gas to lose angular momentum (e.g.

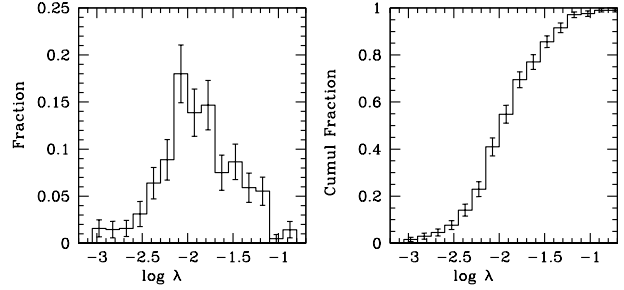


Figure 8. The differential (left) and cumulative (right) distributions of the spin parameters λ derived for the 187 galaxies in our sample with well-measured rotation curves.

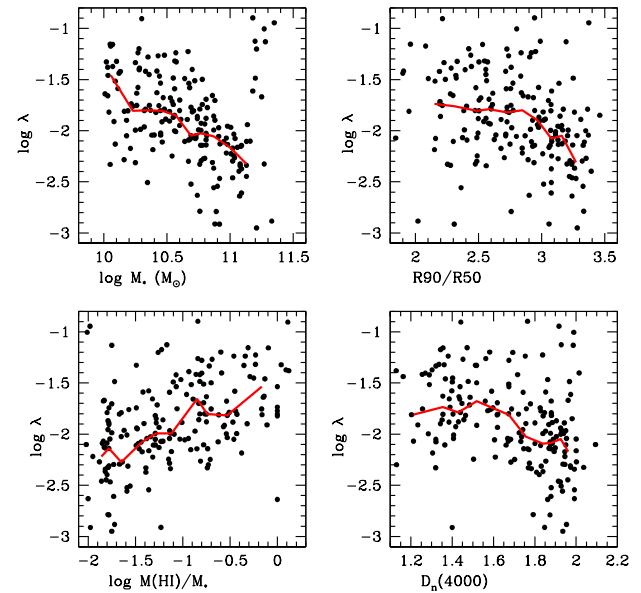


Figure 9. The spin parameter λ is plotted as a function of stellar mass, concentration index, atomic gas mass fraction and 4000 Å break strength. Black points show spin parameter values for individual galaxies, while the red line shows the running median of the spin as a function of these parameters.

Barnes & Hernquist 1996) Interestingly, galaxies with the lowest masses and highest atomic gas mass fractions have a median spin parameter of $\sim 0.03 - 0.04$, which is much more consistent with the predictions of disk formation models where the gas conserves its angular momentum. In addition, we infer from Figure 9 that the scatter in spin parameter for galaxies that are similar in stellar mass, structural parameters and stellar population properties is considerably smaller than the scatter in λ for the population as a whole. Larger samples are needed for accurate estimates of the scatter in λ for galaxies with fixed properties.

4 DARK MATTER HALO PROFILE FITS

In two seminal papers, Navarro, Frenk & White (1996,1997) introduced the concept of a “universal” profile (hereafter

NFW profile) that was able to describe the dark matter density profiles of halos with masses ranging from those of dwarf galaxy halos to those of rich galaxy clusters, independent of the initial density fluctuation spectrum and the values of the cosmological parameters. The NFW profile has the form

$$\frac{\rho(r)}{\rho_{crit}} = \frac{\delta_c}{(r/r_s)(1+r/r_s)^2}, \quad (9)$$

where $r_s = r_{200}/c$ is a characteristic radius and $\rho_{crit} = 3H^2/8\pi G$ is the critical density (H is the current value of the Hubble constant); δ_c and c are two dimensionless parameters, commonly termed the characteristic overdensity and concentration. The virial mass and radius of the halo are defined through the relation $M_{vir} = 200\rho_{crit}(4\pi/3)R_{vir}^3$, and δ_c and c are then linked by the requirement that the mean density within R_{vir} is $200\rho_{crit}$.

Rotation curve fitting is one important way to test whether the NFW profile can fit the dark matter halos of real galaxies. There are many papers in the literature with seemingly contradictory results, but the most recent consensus appears to be that the NFW profile is a reasonably good fit for luminous galaxies (De Blok et al 2008; Martinsson et al 2013), but is a poorer fit for low surface brightness dwarf systems, where the dark matter strongly dominates over the baryonic mass (e.g. Swaters et al 2003). One problem with the interpretation of the results for dwarf galaxies is that because the potential well depth is shallow, feedback effects from bursts of star formation during the formation of the dwarf can in principle affect the dark matter density profile (e.g. Pontzen & Governato 2012).

In this section, we perform NFW halo fits to a subset of 12 galaxies in our sample where the dark matter domination radius $R_{50}(DM) < 0.7R_{50}$. In the Milky Way, dark matter dominates over the baryons at radii larger than ~ 10 kpc, i.e. at around $3R_{50}$. The galaxies that we analyse are thus much more dark-matter dominated than our own Galaxy and as shown in Figure 7, they also tend to have young stellar populations and to be more gas-rich. A detailed analysis of one such a galaxy in our sample, UGC8802 (GASS 35981), was presented in Moran et al (2010). In spite of its high atomic gas content ($2.1 \times 10^{10} M_\odot$), the star formation surface density in this galaxy is low ($\Sigma_{SFR} = 0.003 M_\odot \text{ yr}^{-1} \text{ kpc}^{-2}$) and spread evenly across the galaxy. A sharp drop in metallicity in the outer disk was found in the galaxy, which was later shown to be a common feature of many of the HI-rich galaxies in the sample (Moran et al 2012).

In Figures 10, 11, and 12, we present the NFW halo fits for our 12 selected dark matter-dominated galaxies. The measured values of the rotation velocity are plotted as black circles. The dotted red curves show the contribution from the observed baryons (stars+gas), while the solid red curves show the best fit rotation curve derived from adding the contribution from a NFW halo to the baryons.¹ The parameters of the best-fit NFW model are indicated in the bottom-right corner of each panel.

As can be seen, the rotation curves of these 12 galaxies are regular for the most part, and the NFW halo+observed

¹ We have not attempted to correct for “adiabatic contraction”, the gravitational effect of the central baryonic contribution on the dark matter.

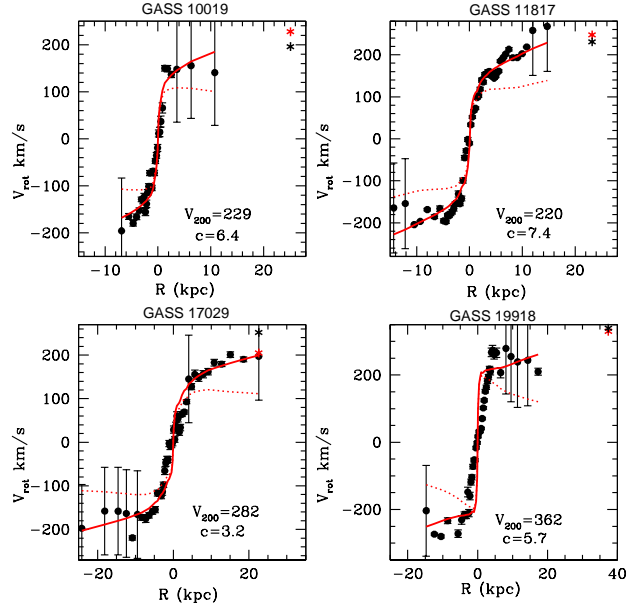


Figure 10. NFW halo fits to the rotation curves of four dark-matter dominated galaxies. The measured values of the rotation velocity are plotted as black circles. The dotted red curves show the contribution from the observed baryons (stars+gas), while the solid red curves show the best fit rotation curve derived from adding the contribution from a NFW halo to the baryons. The HI-profile weighted value of V_{rot} measured from the Arecibo spectrum is plotted as a black star in each panel, while the value inferred from the rotation curve is plotted as a red star.

baryon models provide reasonably good fits to all the galaxies in our sample. There are no cases where the model fails catastrophically and in general the inner power-law region of the rotation curve is well-reproduced. We note that unlike many other studies, we allow no freedom in the assumed mass-to-light ratios for the baryonic component; as described in Section 2, these are derived from fits to the u, g, r, i, z spectral energy distributions, assuming a universal Chabrier (2003) initial mass function. As an additional check, we compare the rotational velocity derived from the width of the 21cm line (see Catinella et al 2012 for details) with the velocity width predicted from weighting the rotation curve by our assumed HI profiles (see section 2). The value measured from the Arecibo spectrum is plotted as a black star in each panel, while the value inferred from the rotation curve is plotted as a red star. As can be seen, the two estimates generally agree to within 10-20% and confirm that our estimates of V_{vir} are reasonably accurate. All the galaxies in our sample are found to reside in quite massive dark matter halos: the smallest (GASS 3591) has a virial velocity of 185 km/s, corresponding to a virial mass of $2 \times 10^{12} M_\odot$. The average value of the halo concentration index c is found to be 9.6 and the 10th-90th percentile range is from 6 to 14. This is in excellent agreement with predictions from Λ CDM cosmological simulations (see Figure 3 of Maccio et al (2007)).

In summary, we conclude that NFW halos provide a good fit to the inner halos of the most dark matter-dominated galaxies in our sample.

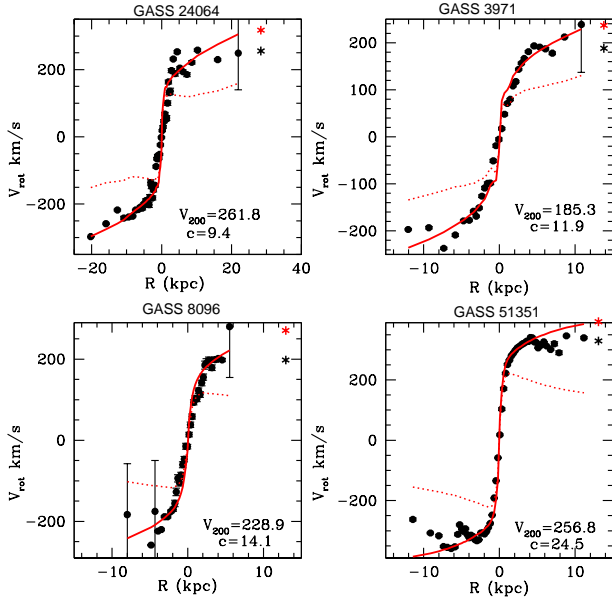


Figure 11. Same as Figure 10, but for 4 more dark-matter dominated galaxies.

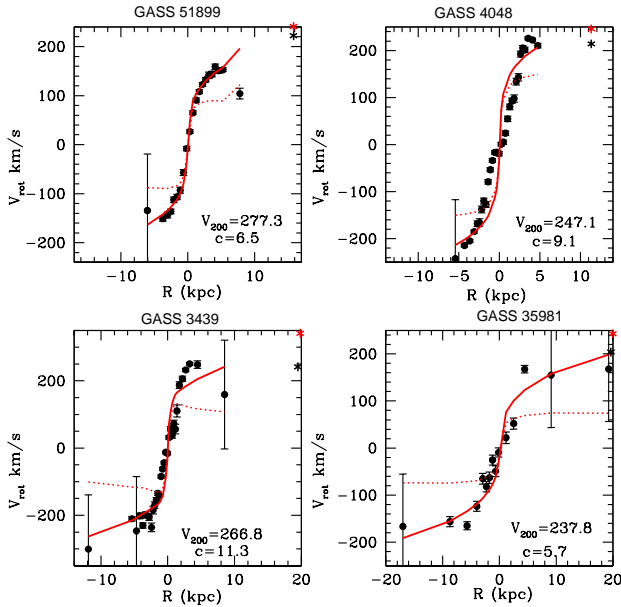


Figure 12. Same as Figure 11, but for 4 more dark-matter dominated galaxies.

5 SUMMARY AND DISCUSSION

The main empirical results of our rotation curve study are the following:

- The inner slopes of the rotation curves correlate more strongly with measures of stellar population age than with galaxy mass or structural parameters. At fixed stellar mass, more actively star-forming galaxies have steeper inner slopes than less actively star-forming galaxies. Another way to

phrase this result is that the ratio of the radius r_s , where the rotation curve transitions away a power-law, to the half-light radius of the galaxy, is smaller in star-forming galaxies than in passive galaxies.

- Galaxies with higher atomic gas mass fractions tend to be more dark-matter dominated than galaxies with low HI content.
- The distribution of spin parameters of the galaxies in our sample shows that the average value of the spin parameter of the galaxies in our sample is ~ 0.01 , which implies that the angular momentum ratio R_j , defined as the ratio between the galaxy specific angular momentum and the total specific angular momentum of its dark matter halo, is less than 1. However, R_j is found to correlate strongly with galaxy mass, structure and gas content. The lowest mass, disk-dominated galaxies with atomic gas mass fractions greater than 20% have median values of R_j of around 1. The highest mass, gas-poor, bulge-dominated galaxies have median values of R_j of 0.1-0.2, i.e. such galaxies have substantially lower specific angular momenta than their host halos.
- The dark matter halo density profiles of the most dark-matter dominated galaxies in our sample are well fit by NFW models. The average concentration parameter is ~ 10 , in good agreement with the predictions of N-body simulations of structure formation in a Λ CDM Universe.

One might first ask whether all of these trends are qualitatively consistent with a picture in which galaxies form by gas cooling and condensation within dark matter halos in a canonical Λ CDM cosmology. In such a picture, the reason why R_j would be less than 1 in some galaxies could be because gas had lost angular momentum and had been channelled inwards in these systems. This inward flow of gas would result in a build-up of higher density gas in the inner regions of the disk, which would then rapidly cool to low temperatures and form bulge stars. Gas that cools and accretes from the surrounding halo is used up more quickly if gas inflows in the disk are common. Frequent inflows would thus be expected to lead to a galaxy that is passive and bulge-dominated. This is a possible explanation of our finding that the spin parameter is smaller in bulge-dominated galaxies with low gas content and old stellar populations.

Gas inflows can arise in two ways: 1) when the disk is perturbed by a merger or interaction with another galaxy, 2) when the disk becomes unstable and forms a bar. The Toomre (1964) disk stability parameter Q is larger in galaxies with higher epicyclic frequencies and larger shear (i.e. larger dV_{rot}/dR). We find that the inner slope of the rotation curve is large in galaxies that are still forming stars, which is consistent with the idea that star formation can be sustained for longer periods if the disk is more stable.

The next step is to test these ideas quantitatively by comparing our results with N-body + hydrodynamical simulations of disk galaxy formation in a Λ CDM Universe in which the cooling of gas in dark matter halos and its subsequent dynamical evolution in disks is treated in a physically self-consistent framework. Well-resolved, dynamically consistent simulations rather than simplified analytic models of disk formation in a hierarchical Universe are also required to predict the effects of feedback processes from supernova and accreting black holes on the inner mass distributions of

galaxies of different types and star formation rates. They will also be very helpful in developing methodology for correcting for asymmetric drift.

There are also hints of more complex dependences of rotation curve shape on star formation history. In Figure 4, we found that galaxies with the very youngest central stellar populations have rotation curves with shallower inner slopes. This hints that supernovae feedback processes occurring during strong central starbursts may be able to alter the inner mass distribution of galaxies. It has been proposed that such mechanisms may be key for resolving the observed rotation curves to dwarf galaxies with the dark matter halo profile predictions of the Cold Dark Matter model. Dynamical studies of larger galaxy samples observed using integral field spectrographs spanning a wider range of masses and redshifts will shed more light this issue.

ACKNOWLEDGMENTS

We thank Simon White for helpful discussions.

REFERENCES

- Barnes J. E., Hernquist L., 1996, *ApJ*, 471, 115
 Bett P., Eke V., Frenk C. S., Jenkins A., Helly J., Navarro J., 2007, *MNRAS*, 376, 215
 Bigiel F., Blitz L., 2012, *ApJ*, 756, 183
 Böhm A., et al., 2004, *A&A*, 420, 97
 Broeils A. H., Rhee M.-H., 1997, *A&A*, 324, 877
 Bruzual G., Charlot S., 2003, *MNRAS*, 344, 1000
 Catinella B., et al., 2010, *MNRAS*, 403, 683
 Catinella B., et al., 2012, *MNRAS*, 420, 1959
 Chabrier G., 2003, *PASP*, 115, 763
 Combes F., 2002, *NewAR*, 46, 755
 de Blok W. J. G., Walter F., Brinks E., Trachternach C., Oh S.-H., Kennicutt R. C., Jr., 2008, *AJ*, 136, 2648
 Donato F., et al., 2009, *MNRAS*, 397, 1169
 Dutton A. A., van den Bosch F. C., 2012, *MNRAS*, 421, 608
 Fu J., Guo Q., Kauffmann G., Krumholz M. R., 2010, *MNRAS*, 409, 515
 Guo Q., et al., 2011, *MNRAS*, 413, 101
 Kormendy J., Freeman K. C., 2004, *IAUS*, 220, 377
 Macciò A. V., Dutton A. A., van den Bosch F. C., Moore B., Potter D., Stadel J., 2007, *MNRAS*, 378, 55
 Martin C. L., 2005, *ApJ*, 621, 227
 Martinsson T. P. K., Verheijen M. A. W., Westfall K. B., Bershadsky M. A., Schechtman-Rook A., Andersen D. R., Swaters R. A., 2013, *A&A*, 557, AA130
 Martinsson T. P. K., Verheijen M. A. W., Westfall K. B., Bershadsky M. A., Andersen D. R., Swaters R. A., 2013, *A&A*, 557, AA131
 Moran S. M., Miller N., Treu T., Ellis R. S., Smith G. P., 2007, *ApJ*, 659, 1138
 Moran S. M., et al., 2010, *ApJ*, 720, 1126
 Moran S. M., et al., 2012, *ApJ*, 745, 66
 Moster B. P., Naab T., White S. D. M., 2013, *MNRAS*, 428, 3121
 Navarro J. F., Frenk C. S., White S. D. M., 1996, *ApJ*, 462, 563
 Navarro J. F., Frenk C. S., White S. D. M., 1997, *ApJ*, 490, 493
 Noordermeer E., van der Hulst J. M., Sancisi R., Swaters R. S., van Albada T. S., 2007, *MNRAS*, 376, 1513
 Persic M., Salucci P., Stel F., 1996, *MNRAS*, 281, 27
 Pontzen A., Governato F., 2012, *MNRAS*, 421, 3464
 Saintonge A., et al., 2011, *MNRAS*, 415, 32
 Salim S., et al., 2005, *ApJ*, 619, L39
 Sofue Y., Tutui Y., Honma M., Tomita A., Takamiya T., Koda J., Takeda Y., 1999, *ApJ*, 523, 136
 Sofue Y., Rubin V., 2001, *ARA&A*, 39, 137
 Spano M., Marcellin M., Amram P., Carignan C., Epinat B., Hernandez O., 2008, *MNRAS*, 383, 297
 Swaters R. A., Madore B. F., van den Bosch F. C., Balcells M., 2003, *ApJ*, 583, 732
 Toomre A., 1964, *ApJ*, 139, 1217
 Wang J., et al., 2013, *MNRAS*, 433, 270
 Wang J., et al., 2014, *MNRAS*, 441, 2159
 Weinmann S. M., Kauffmann G., von der Linden A., De Lucia G., 2010, *MNRAS*, 406, 2249
 York D. G., et al., 2000, *AJ*, 120, 1579